# Modeling with Rational Biquadratic Splines

K. Karčiauskas[1] and J. Peters[2] [1]Vilnius University, [2]CISE, U of Florida, Gainesville, FL 32611, USA

**Abstract**

We develop a rational biquadratic $G^1$ analogue of the non-uniform $C^1$ B-spline paradigm. These $G^1$ splines can exactly reproduce parts of multiple basic shapes, such as cyclides and quadrics, and combine them into one smoothly-connected structure. This enables a design process that starts with basic shapes, re-pepresents them in spline form and uses the spline form to provide shape handles for localized free-form modification that can preserve, in the large, the initial fair, basic shapes.

*Key words:* rational spline, geometric continuity, quadratic, reproduction, cyclide, quadric, surface of revolution, free-form, design

## 1. Introduction

We introduce a simple, yet surprisingly rich set of rational biquadratic $G^1$ spline constructions. The resulting class of surfaces can replicate pieces of quadrics and cyclides as parts of a *free-form* spline complex. This combination of reproduction and smoothness improves on classical $C^1$ biquadratic NURBS, which provide smoothness only, and formulas for the rational Bézier form that provide exact representation of individual pieces only. And they give a practical application of the classical discussion of smoothness constraints for rational spline curves, e.g. [Boe87,GB88,Bar93]. The design workflow proposed below emphasises that the control net is no longer the primary creation tool. The net and its rational weights are initialized by the designer's choice of basic shapes. Manipulating this initialized net allows localized free-form design. In full analogy to standard splines, we derive the rational biquadratic splines as a tensor-product of a curve construction and then enrich it to include sphere-like shapes and quadrics.

## 2. Rational quadratic $G^1$ curves

As illustrated in Fig. 1, the control structure of our rational quadratic $G^1$ curves extends that of quadratic $C^1$ NURBS [Far88,PBP02]. It consists of

– the *affine* B-spline-like control points $\mathbf{p}^i \in \mathbb{R}^d$. For example, the dimension is $d = 2$ for planar curves. We will also use $d = 3$ for surface representation in 3-space and $d = 4$ for construction in projective space; we use $d = 1$ when we discuss the coordinate functions of the construction.

– the parameters $\beta_i > 0$ of $G^1$ continuity between consecutive rational quadratic segments $\mathbf{f}_{i-1}$ and $\mathbf{f}_i$ and

– the (inner) weights, $w_i > 0$ of segment $\mathbf{f}_i$.

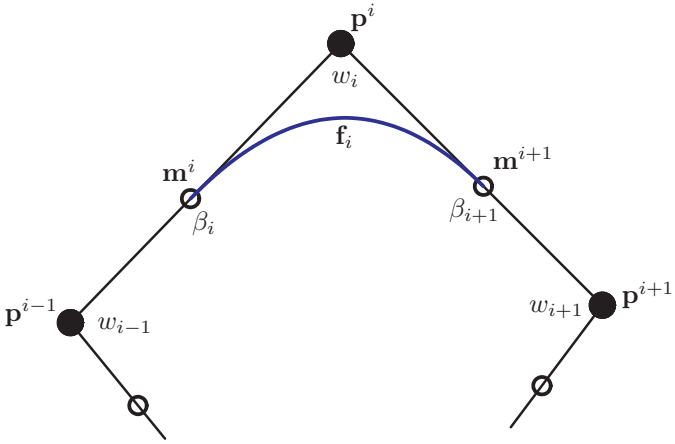


Fig. 1. Control structure and scalars defining a rational quadratic $G^1$ spline curve with pieces $\mathbf{f}_i$ defined by affine Bézier control points $\mathbf{m}^i$, $\mathbf{p}^i$, $\mathbf{m}^{i+1}$ and a middle weight $w_i$ and a parameter $\beta_i$.

This control structure, itself initialized by the design workflow below, defines the pieces of degree 2 in rational Bernstein-Bézier form $\mathbf{f}_i : [0..1] \to \mathbb{R}^d$ with affine coefficients $\mathbf{b}^i_k \in \mathbb{R}^d$

$$\mathbf{f}_i(u) := \frac{\sum_{k=0}^2 w^i_k \mathbf{b}^i_k B^2_k(u)}{\sum_{k=0}^2 w^i_k B^2_k(u)}, \qquad (1)$$
$$B_k(u) := \binom{2}{k}(1-u)^{2-k}u^k.$$

The construction (3) in Theorem 1 below shows how the affine coefficients $\mathbf{b}^i_k \in \mathbb{R}^d$ and scalar weights $w^i_k$ are derived from the control structure so that $\mathbf{f}_{i-1}$ and $\mathbf{f}_i$ *join* $G^1$ at the common point $\mathbf{f}_{i-1}(1) = \mathbf{f}_i(0)$, i.e. so that, for a scalar $\beta_i > 0$,

$$\mathbf{f}'_i(0) = \beta_i \mathbf{f}'_{i-1}(1). \qquad (2)$$

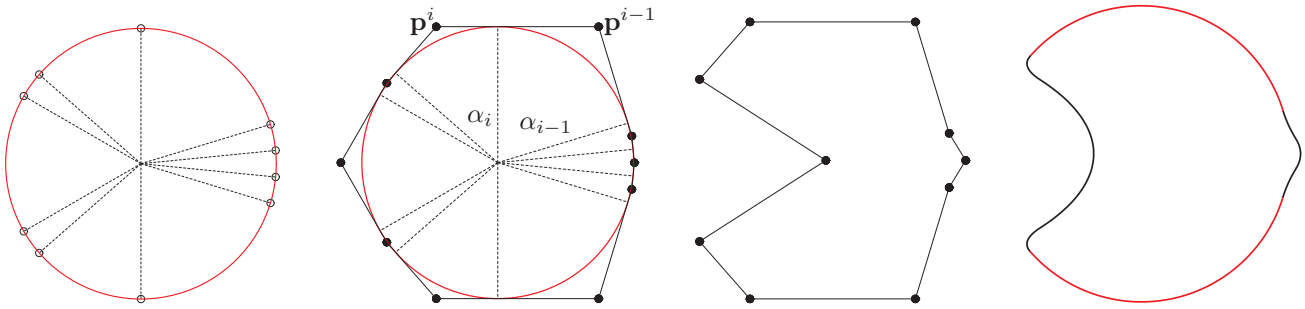


(a) designer (b) algorithm (c) designer (d) algorithm

Fig. 2. Design work-flow for modeling with circle pieces as rational quadratic splines. (a) The designer partitions the circle; (b) the algorithm creates the control net $\mathbf{p}^i$ and sets the parameters $\beta_i, w_i$; (c) the designer modifies the net; (d) the algorithm creates the curve using (3) so that the red portion remains on the circle.

This stretching of first-order derivatives can represent non-uniform B-spline knot-sequences when we express the splines piecemeal in Bézier form and set $\beta_i := \frac{u_{i+1}-u_i}{u_i-u_{i-1}}$ for a knot equence $u_{i-1} < u_i < u_{i+1}$ [Joe89]. (However, given the $\beta_i$, the equations for finding the knots of a non-uniform periodic spline generically have no admissible solution.)

**Theorem 1** *If $\mathbf{f}_{i-1}$, $\mathbf{f}_i$ are rational quadratic curves with Bézier control points $\mathbf{b}_1^i := \mathbf{p}^i$, $\mathbf{b}_2^{i-1} = \mathbf{b}_0^i := \mathbf{m}^i$ and $w_1^i := w_i$, $w_0^i = w_2^i = 1$,*

$$\mathbf{m}^i := (1-\mu_i)\mathbf{p}^{i-1} + \mu_i \mathbf{p}^i, \quad \mu_i := \frac{w_i}{w_{i-1}\beta_i + w_i} \tag{3}$$

*then $\mathbf{f}_i'(0) = \beta_i \mathbf{f}_{i-1}'(1)$.*

**Proof** Since

$$\mathbf{f}_{i-1}'(1) = 2\left((\mathbf{m}^i - w_{i-1}\mathbf{p}^{i-1}) - (1-w_{i-1})\mathbf{m}^i\right),$$
$$\mathbf{f}_1'(0) = 2\left((w_i\mathbf{p}^i - \mathbf{m}^i) - (w_i - 1)\mathbf{m}^i\right),$$

the claim amounts to showing

$$\beta_i(-w_{i-1}\mathbf{p}^{i-1} + w_{i-1}\mathbf{m}^i) = w_i\mathbf{p}^i - w_i\mathbf{m}^i,$$

which holds due to (3). |||

### 2.1. *Circular arcs, control net from shape and design*

In particular, as illustrated in Fig. 2 (a), arcs $\mathbf{f}_i$ of a circle with the opening angles $\alpha_i$ can be represented in our rational quadratic Bézier form with its end-weights equal to 1. Starting with points $\mathbf{m}^i$ on the circle with center $(0,0)$, we obtain the spline coefficients of the circle as

$$\mathbf{p}^i := \frac{1}{1+\cos\alpha_i}(\mathbf{m}^i + \mathbf{m}^{i+1}). \tag{4}$$

In effect, this yields a *reverse process* to (3). Since rational quadratics parameterize circle arcs by chord length [Far06], we obtain rational $G^1$ splines with

$$w_i := \cos\frac{\alpha_i}{2} \quad \text{and} \quad \beta_i := \frac{\sin\frac{\alpha_i}{2}}{\sin\frac{\alpha_{i-1}}{2}}. \tag{5}$$

We note for later use, that, since we can express the circle, we can express $\cos$ and $\sin$ terms in our $G^1$ spline form. Generally, any tangent continuous, rational quadratic spline curve with positive weights can be converted to the rational $G^1$ spline form of Theorem 1: The curve pieces in Bézier form (1) are normalized and reparametrized so that $w_0^i = w_2^i = 1$. Then tangent continuity allows enforcing (3) by choice of $\mu_i$ and $\beta_i$.

Fig. 2 illustrates the proposed *design work-flow* later extended to tensor-product constructions. Starting with a circle, a designer marks points $\mathbf{m}^i$ in (a), or, alternatively, a starting angle and angle increments $\alpha_i$, to prepare the design for localized change. Applying the reversing process (4), (5), the algorithm computes the control net $\mathbf{p}^i$ (see (b)) and sets the parameters $\beta_i, w_i$. The designer then freely modifies the net locally as in (c). Finally the algorithm re-creates the curve using (3) so that, as in (d), the segments, that are not among the three related to each moved control point, remain on the circle.

## 3. Biquadratic $G^1$ splines

We tensor the curve construction to derive control points $\mathbf{b}_{rs}^{ij} \in \mathbb{R}^d$ and weights $w_{rs}^{ij}$ of biquadratic patches $\mathbf{f}^{ij}$ that are controlled by a regular quadrilateral grid of (B-spline-like) control points $\mathbf{p}^{ij} \in \mathbb{R}^d$ — with associated scalars $\dot{w}_r^i$, $\dot{\beta}_i$ in the $u$-direction and scalars $\ddot{w}_s^j$, $\ddot{\beta}_j$ in the $v$-direction.

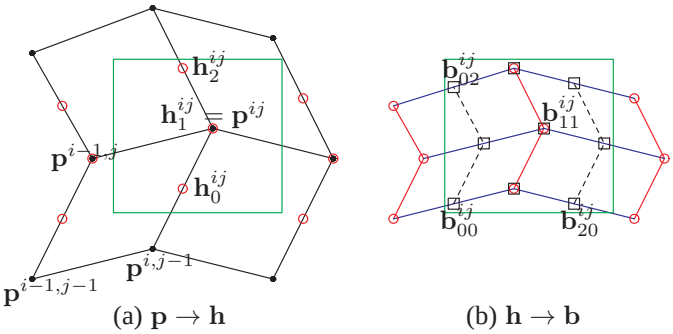


(a) $\mathbf{p} \to \mathbf{h}$ (b) $\mathbf{h} \to \mathbf{b}$

Fig. 3. Bi-quadratic construction of Theorem 2. The green square roughly outlines the extent of one resulting patch.

**Theorem 2** *Rational biquadratic functions $\mathbf{f}^{ij} : [0..1]^2 \to \mathbb{R}^d$,*

$$\mathbf{f}^{ij} := \frac{\sum_{r=0}^2 \sum_{s=0}^2 w_{rs}^{ij}\mathbf{b}_{rs}^{ij} B_r^2(u) B_s^2(v)}{\sum_{r=0}^2 \sum_{s=0}^2 w_{rs}^{ij} B_r^2(u) B_s^2(v)} \tag{6}$$

*form a $G^1$ spline complex if we set weights and control points by the following* **Biquadratic Construction:** *(cf. Fig. 3)*

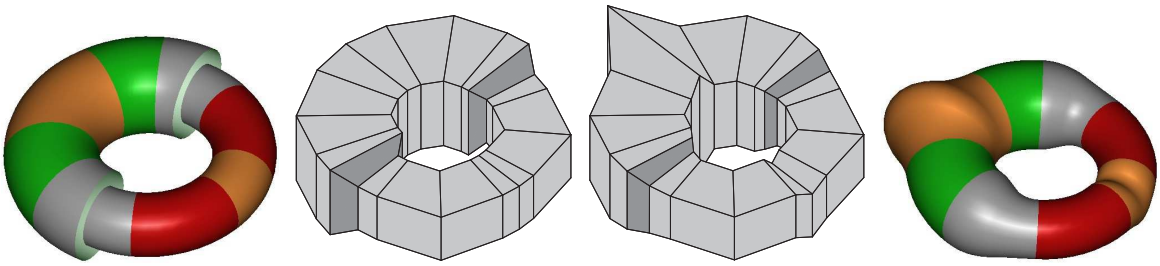

(a) designer (b) algorithm (c) designer (d) algorithm

Fig. 4. Surface design work-flow: (a) designer marks regions of the two torus halves. The regions will serve as either transitions (gray), for later modification (orange) or remain on the torus (green, red). The modification regions are partitioned into three equal sub-sectors, transition regions into two. The algorithm creates the control net $\mathbf{p}^{ij}$ and sets the parameters $\dot{w}_r^i$, $\dot{\beta}_i$ and $\ddot{w}_s^j$, $\ddot{\beta}_j$. (c) the designer modifies the net. The transition between the torus pieces has been tempered as in Fig. 7; (d) the algorithm creates the surface using the formulas of Theorem 2.

*set* $w_{rs}^{ij} := \dot{w}_r^i \ddot{w}_s^j$, $\dot{\mu}_i$ *for the* $u$*-direction and* $\ddot{\mu}_j$ *for* $v$*-direction as in* (3),

$$\mathbf{h}_0^{ij} := (1-\ddot{\mu}_j)\mathbf{p}^{i,j-1} + \ddot{\mu}_j \mathbf{p}^{ij},\ \mathbf{h}_2^{i,j-1} := \mathbf{h}_0^{ij}\ ,\ \mathbf{h}_1^{ij} := \mathbf{p}^{ij},$$

*and then for the other direction*

$$\mathbf{b}_{0s}^{ij} := (1-\dot{\mu}_i)\mathbf{h}_s^{i-1,j} + \dot{\mu}_i \mathbf{h}_s^{ij}\ ,\ \mathbf{b}_{2s}^{i-1,j} := \mathbf{b}_{0s}^{ij}\ ,\ \mathbf{b}_{1s}^{ij} := \mathbf{h}_s^{ij}.$$

The result is unchanged if we reverse the ordering of directions.

*Proof* We show for the $u$-derivative $\partial_u \mathbf{f} := \frac{\partial f}{\partial u}$ that

$$\partial_u \mathbf{f}^{ij}(0,v) = \dot{\beta}_i \partial_u \mathbf{f}^{i-1,j}(1,v).$$

Then $\partial_v \mathbf{f}^{ij}(u,0) = \ddot{\beta}_j \partial_v \mathbf{f}^{i,j-1}(u,1)$ follows from the analogous argument. Since $w_{rs}^{ij} := \dot{w}_r^i \ddot{w}_s^j$,

$$\sum_{r=0}^{2}\sum_{s=0}^{2} w_{rs}^{ij} B_r^2(u) B_s^2(v) = \sum_{r=0}^{2} \dot{w}_r^i B_r^2(u) \sum_{s=0}^{2} \ddot{w}_s^j B_s^2(v). \quad (7)$$

Let $j$ be fixed and define $\bar{w}_k(v) := \ddot{w}_k^j B_k^2(v) / \sum_{s=0}^2 \ddot{w}_s^j B_s^2(v)$. Then $\sum_k^2 \bar{w}_k(v) = 1$ and

$$\mathbf{f}^{ij}(u,v) := \frac{\sum_{r=0}^2 \dot{w}_r^i \big(\sum_{s=0}^2 \bar{w}_s(v) \mathbf{b}_{rs}^{ij}\big) B_r^2(u)}{\sum_{r=0}^2 \dot{w}_{ir} B_r^2(u)}\ .$$

With the abbreviations

$$\overline{\mathbf{b}}_{ir}(v) := \sum_{s=0}^{2} \bar{w}_s(v) \mathbf{b}_{rs}^{ij}\ ,\ \overline{\mathbf{p}}_i(v) := \sum_{s=0}^{2} \bar{w}_s(v) \mathbf{p}_s^{ij}\ ,$$

$$\mathbf{f}^{ij}(u,v) = \frac{\sum_{r=0}^2 \dot{w}_r^i \overline{\mathbf{b}}_{ir}(v) B_r^2(u)}{\sum_{r=0}^2 \dot{w}_r^i B_r^2(u)},$$

$$\overline{\mathbf{b}}_{i0}(v) = (1-\dot{\mu}_i)\overline{\mathbf{p}}_{i-1}(v) + \dot{\mu}_i \overline{\mathbf{p}}_i(v)\ ,$$

$$\overline{\mathbf{b}}_{i-1,2}(v) = \overline{\mathbf{b}}_{i0}(v)\ ,\ \overline{\mathbf{b}}_{i1}(v) = \overline{\mathbf{p}}_i(v).$$

The proof then follows from Theorem 1. *End of proof*

Using (7) and following the steps of tensoring procedure, we get the important Corollary 1.

**Corollary 1** *Considering one coordinate at a time* ($d = 1$)*, let* $\mathbf{f}_i(u)$ *be a rational quadratic piece of a* $G^1$ *spline with control points* $\dot{\mathbf{p}}_i$ *as in Theorem 1; and let* $\mathbf{g}_j(v)$ *be another piece with control points* $\ddot{\mathbf{p}}_j$*.*
*(a) Then the functions* $\mathbf{f}^{ij}(u,v) := \mathbf{f}_i(u)\mathbf{g}_j(v)$ *form a bi-quadratic* $G^1$ *spline with control points* $\mathbf{p}^{ij} := \dot{\mathbf{p}}_i \ddot{\mathbf{p}}_j$*.*
*(b) If all* $\mathbf{p}^{ij} := 1$ *then* $\mathbf{f}^{ij} = 1$*.*

## 4. Reproducing classical shapes

A number of basic, classical shapes have a trigonometric representation in real projective 3-space as $(\tau_1, \tau_2, \tau_3, \tau_4) \in \mathbb{P}^3$. The torus and cyclides are in the family

$$\begin{aligned}\tau_k :=& a_{k0} + a_{k1}\cos u + a_{k2}\sin u + a_{k3}\cos v + a_{k4}\sin v \\ &+ (a_{k5}\cos u + a_{k6}\sin u)\cos v \\ &+ (a_{k7}\cos u + a_{k8}\sin u)\sin v, \qquad k = 1,2,3,4,\end{aligned} \quad (8)$$

(see e.g. [DMP93]) and all quadric surfaces except for the hyperbolic paraboloid are in the family

$$\tau_k := \sum_{l=0}^{2} (a_{kl0} + a_{kl1}\cos u + a_{kl2}\sin u) v^l. \quad (9)$$

For example, a cyclide may be parameterized in the form (8) by choosing the nonzero $a_{ki}$ to be

$$\begin{aligned} a_{10} := \mu\mathsf{s},\ a_{11} := a\mathsf{c}^2,\ a_{15} := -\mu,\ a_{22} := a\mathsf{c}\ a_{26} := -\mu\mathsf{c}, \\ a_{34} := -\mu\mathsf{c},\ a_{37} := a\mathsf{cs},\ a_{40} := 1,\ a_{45} := -\mathsf{s}, \\ \mathsf{c} := \cos\gamma, \mathsf{s} := \sin\gamma, \end{aligned}$$

where $\gamma$ is fixed to match the general form in [DMP93]. If additionally $a = 2$, $\mu = 1$, $\gamma = 0$, we get the radius 2 torus with unit circle sections:

$$[(2-\cos v)\cos u, (2-\cos v)\sin u, -\sin v, 1].$$

To parameterize (8) in spline form, we represent its cos-sin-pairs piecemeal as rational quadratics as in Section 2.1. That is, we choose, first in the $u$-direction, a partition represented by angles $\dot{\eta}_i$ starting with some free-to-choose but fixed parameter $u = u_0$ and set

$$\mathbf{p}_1^i := \frac{1}{\cos\frac{\dot{\alpha}_i}{2}} \begin{bmatrix} \cos(\dot{\eta}_{i-1} + \frac{\dot{\alpha}_i}{2}) \\ \sin(\dot{\eta}_{i-1} + \frac{\dot{\alpha}_i}{2}) \end{bmatrix}, \quad \dot{\alpha}_i := \dot{\eta}_i - \dot{\eta}_{i-1}, \quad (10)$$

where $\dot{\alpha}_i$ are the opening angles. Analoguously, we choose a partition $\ddot{\eta}_j$ and $\mathbf{p}_1^j$ in the $v$-direction. Equation (5) defines the scalars $\dot{\beta}_i$, $\dot{w}_i$, $\ddot{\beta}_j$, $\ddot{w}_j$. Now Corollary 1 applies.

To parameterize (9) in spline form, the $u$-direction is treated as for (8), and $v^s$ is converted to a $C^1$ spline with knot sequence $\{v_j\}$, $\ddot{\beta}_j := \frac{v_j - v_{j-1}}{v_{j-1} - v_{j-2}}$, and weights equal 1; hence $w_{rs}^{ij} = \dot{w}_r^i$. Then Corollary 1 applies.

*Biquadratic homogeneous* parameterizations, including the hyperbolic paraboloid, are treated analogously, with non-uniform biquadratic polynomial splines as a special case. Here we simply set all weights to 1 and all scalars $\dot\beta_i$, $\ddot\beta_j$ to the ratio of the lengths of consecutive knot intervals [Joe89]. The control mesh is the spline control net.

*Surfaces of revolution* are naturally parameterized by rotating a *profile curve*, e.g. a $G^1$ curve spline $f(v) := [x(v), 0, z(v)]$, around the $z$-axis (c.f. Fig. 23 (a)). For simplicity, we assume that the profile is in the plane containing the axis of rotation. A corresponding parameterization is

$$[x(v)\cos u, x(v)\sin u, z(v), 1] \in \mathbb{R}^4. \qquad (11)$$

This can be represented as in Corollary 1: the profile provides the $v$-spline and formulas (5) and (10) define the spline in $u$. Fig. 23 (b) and (c) make the point that while standard modeling with surfaces of revolution allows only modification of the profile, our rational quadratic $G^1$ splines invite free-form modifications.

*Trigonometric modeling*: We can not expect the designer to work directly with $(\cos, \sin)$-parametrizations even though such modeling, followed by the automatic conversion to rational biquadratic $G^1$ splines, would open up another set of elegant shapes. Fig. 8 shows two such $C^\infty$ shapes that fall outside the usual list of basic shapes. Shapes as in Fig. 8 would be difficult, if not impossible, to design by starting with a cyclide and adding deformations. *Villarceau*-parameterization of the torus Fig. 9,*left*, distributes control points and hence shape handles Fig. 9,*right*, differently from, say, Fig. 4 or Fig. 7. Similarly, *cylinders* allow redistributing the control net along the axes so that, e.g., direct smooth transitions between torus and cylinder are possible as illustrated in Fig. 21 (b). Our suggestion is to create a design interface that offers families of such initial shapes and meshes to the practitioner for further editing.

**From 4-tuples of $\mathbf{G^1}$ splines to 3-tuples of $\mathbf{G^1}$ splines.** In all the above cases, we have classic shapes represented as 4-tuples of rational $G^1$ splines with pieces $\mathbf{f}_k^{ij} := \frac{\varphi_k^{ij}}{\phi^{ij}}$, $k = 1, 2, 3, 4$ of the form (6) (and identical denominator $\phi^{ij}$ per piece, hence no subscript $k$). For each coordinate $k$, $\mathbf{f}_k^{i-1,j}$ and $\mathbf{f}_k^{ij}$ join $G^1$ with identical scalar $\dot\beta_i > 0$ and similarly in the $v$-direction. Now we use the fact that if $\hat g$ and $\hat h$ join $G^1$ with scalar $\beta$, and $g$ and $h$ join $G^1$ with the same scalar $\beta$, then $\frac{\hat g}{g}$ and $\frac{\hat h}{h}$ join $G^1$ with scalar $\beta$. This implies that also the 3-tuples of rational pieces $\frac{\mathbf{f}_k^{ij}}{\mathbf{f}_4^{ij}} = \frac{\varphi_k^{ij}}{\varphi_4^{ij}}$, $k = 1, 2, 3$, join to form a rational $G^1$ spline.

## 5. Design with $G^1$ splines

As illustrated in Fig. 4, the design work-flow carries over from the curve setting of Fig. 2 to the surface setting: the designer selects and positions the basic shapes and marks regions in anticipation of modifications; the algorithm of Section 4 then creates the control net $\mathbf{p}^{ij}$ and sets the parameters $\dot w_r^i$, $\dot\beta_i$ and $\ddot w_s^j$, $\ddot\beta_j$. Then the designer can change the shape as usual by manipulating control points and weights

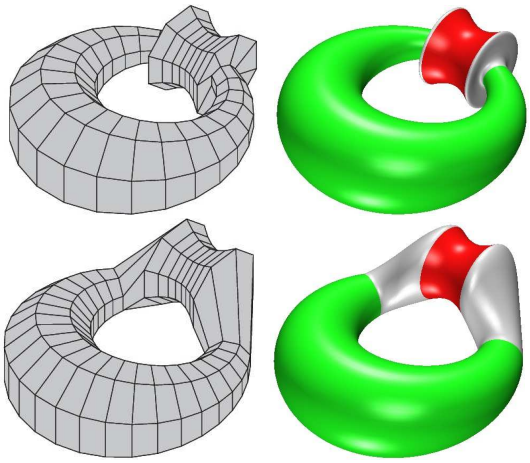

Fig. 5. One spline combining a cyclide (green) and a one-sheeted hyperboloid (red).

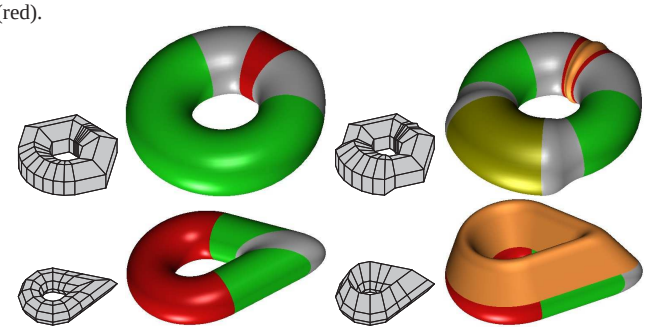

Fig. 6. Splines combining torus and cylinder pieces to something more interesting.

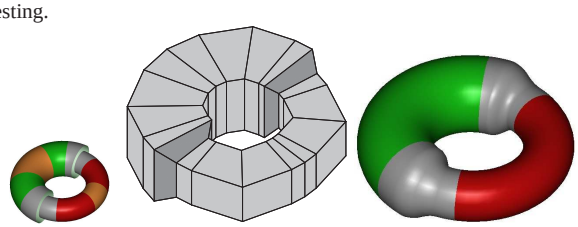

(a) input (b) direct transition

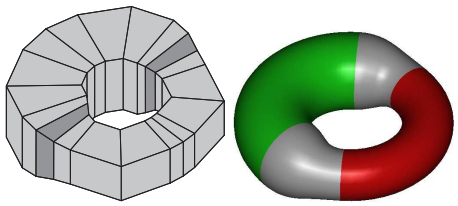

(c) tempered transition

Fig. 7. Transition adjustment (cf. Fig. 4): (a) Input marked up for design changes. The transition areas are grey. (b) Direct transition of the control meshes of the two torus halves. (c) Tempered transition without adding control points: only the vertices of the dark quads are modified.

$$\mathbf{a}^{ij} := \left(\frac{\mathbf{p}_1^{ij}}{\mathbf{p}_4^{ij}}, \frac{\mathbf{p}_2^{ij}}{\mathbf{p}_4^{ij}}, \frac{\mathbf{p}_3^{ij}}{\mathbf{p}_4^{ij}}\right) \in \mathbb{R}^3, \qquad \hat W^{ij} := \mathbf{p}_4^{ij}. \qquad (12)$$

The algorithm reverses (12) to obtain, from $\mathbf{a}^{ij}$ and $\hat W^{ij}$, the modified 4-tuple $\mathbf{p}^{ij}$; and the Biquadratic Construction of Theorem 2 generates the smooth surface.

In the examples of Fig. 5, Fig. 6 and Fig. 7, parts of the $G^1$ meshes $\mathbf{p}^{ij}$ of several basic shapes are merged into one $G^1$

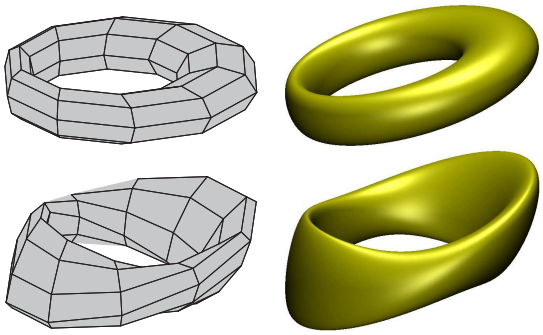

Fig. 8. Design with trigonometric parameterizations.

Fig. 9. A Villarceau parameterization of the torus offers different mesh layout and hence manipulation handles compared to Fig. 4 or 6.

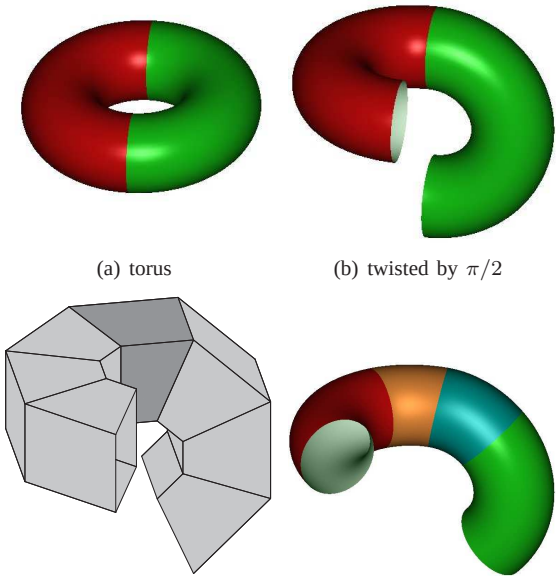

(a) torus (b) twisted by $\pi/2$

(c) control net from (b) (d) $G^1$ spline

Fig. 10. (a) A uniformly partitioned torus is (b) opened and twisted. The result is still a $C^1$ surface. The initial uniform partition of (b) induces the control net (c): all data corresponding to light grey are defined by the torus pieces. The control net (c) yields the rational biquadratic $G^1$ spline surface (d): the red and the green pieces are exactly on the torus pieces of (b).

mesh, without adding control points. While more subtle transitions can potentially be designed by adding transition layers, the examples show that even straightforward use of new spline representation yields satisfactory results. Fig. 22 shows similar designs combining quadrics.

*Limitations* In the curve case, every tangent continuous object can be transformed into our rational $G^1$ spline representation. In the surface case, we restricted ourselves to tensored constructions. Therefore not every tangent plane continuous rational biquadratic patchwork can be represented in our spline form. For example, the twisted half-tori in Fig. 10 (b) join smoothly since they share the same tangent cylinder. The torus pieces of (b) induce the control polyhedron Fig. 10 (c) and all parameters $\dot{w}^i_r$, $\dot{\beta}_i$ and $\ddot{w}^j_s$, $\ddot{\beta}_j$ except possibly $\dot{\beta}_i$ of the dark grey segments. That is $\dot{\beta}_i = \ddot{\beta}_j = 1$. Symmetry then also forces the $\dot{\beta}_i$ of the dark grey segments to be 1. Applying the Biquadratic Construction of Theorem 2 to these data yields (d) which is subtly different from (b) at the transition between the pieces. (The surface (d) is also shorter by the end segments. The ends are not fully defined by the control net (c), but, as torus pieces, can be represented by extending the control net). Since both solutions are smooth, why would one choose one over the other? The advantage of (b) is that it has as rational offset [Pra89] while (d) has not. The advantage of (d) is that the surface will stay $G^1$ even after local redesign, whereas the approach in (b) will not.

## 6. Free-form spheres

We model the sphere as a collection of biquadratic patches with a regular tensor-product control mesh. The poles are boundaries collapsed into a point as illustrated in Fig. 11. The fan of triangles surrounding the collapsed point is called a *polar configuration* [KP07].

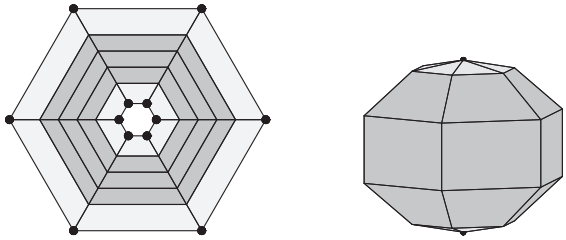

(a) polar mesh unfolded and poles split (b) polar mesh

Fig. 11. Mesh with two polar configurations.

To exactly reproduce a sphere, we reparameterize the inverse stereographic projection

$$\mathbf{s}^{-1} := (2x, 2y, 1 - x^2 - y^2, 1 + x^2 + y^2) \text{ by}$$
$$(x, y) = \rho(u, v) := \Big(\frac{1-v}{v}\cos u, \frac{1-v}{v}\sin u\Big), \qquad (13)$$

the parameterization of the punctured plane. That is, we form $v^2\mathbf{s}^{-1}(\rho)$ where multiplication by $v^2$ clears the common denominator of the 4-tuple, $v = 0$ corresponds to south pole and $v = 1$ to the north pole and $u$ to the latitudinal direction.

**Free-form design with sphere parts.** Fig. 12 (b) displays the control points $\mathbf{p}^{ij} = \mathbf{b}^{ij}_{11}$ of the $G^1$ spline near the pole. Symbolic calculation shows that the lines through pairs $\mathbf{p}^{i1}$ and $\mathbf{p}^{i2}$ intersect at one point $\mathbf{p}^{pole}$ Fig. 12 (d). Conversely, for a constant $\sigma$ independent of $i$, $\mathbf{p}^{i1} = (1-\sigma)\mathbf{p}^{i2} + \sigma\mathbf{p}^{pole}$. Therefore a designer can manipulate the mesh shown in Fig. 11 (b), and we can restore the points $\mathbf{p}^{i1}$ in (d) from $\mathbf{p}^{i2}$ and $\mathbf{p}^{pole}$. The procedure of Theorem 2 then creates all layers of the sphere (grey in (c)) except for the pole caps.

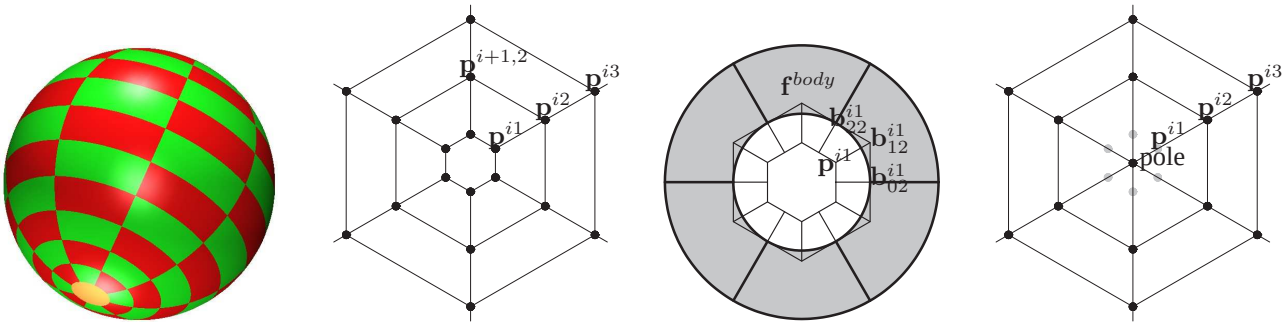


(a) sphere (b) control points $\mathbf{p}^{ij} = \mathbf{b}_{11}^{ij}$ (c) grey = layers on sphere; control-net = $\partial\mathbf{f}^{body}$ (d) $\mathbf{p}^{i1} = (1-\sigma)\mathbf{p}^{i2} + \sigma\mathbf{p}^{pole}$

Fig. 12. **Sphere:** (b) Bi-quadratic polar mesh $\mathbf{p}^{ij}$ with circular index $i$ and $j = 0$ for the south pole. (c) shows Bézier coefficients of the affine 1-jet $\partial\mathbf{f}^{body}$ resulting from the Biquadratic Construction with $\mathbf{b}^{i1} := \mathbf{p}^{i1}$ (the construction yields patches with the pole layer missing). (d) construction of the pole.

**General Polar Caps.** To construct free-form caps at the poles, assume that the south-to-north direction is parameterized by $v$ with the knot sequence $[0, v_1, v_2, \ldots, v_{m-1}, v_m, 1]$, that $\mathbf{p}^{south}$ corresponds to $v = 0$ and $\mathbf{p}^{north}$ to $v = 1$. If we associate the mesh layer surrounding $\mathbf{p}^{south}$ with $v_2$ and the one surrounding $\mathbf{p}^{north}$ with $v_{m-1}$, we can add an interim layer at $v_1$ (south) and one for $v_m$ (north) as

$$\begin{aligned}\mathbf{p}^{i1} :=& (1-\sigma^{south})\mathbf{p}^{i2} + \sigma^{south}\mathbf{p}^{south}\ ,\\ \mathbf{p}^{im} :=& (1-\sigma^{north})\mathbf{p}^{i,m-1} + \sigma^{north}\mathbf{p}^{north}.\end{aligned}$$

If we set the polar control points and constants as

$$\begin{aligned}\mathbf{p}^{south} :=& (0, 0, \frac{1-2v_1+2v_1^2}{2v_1-1}, 1),\\ \sigma^{south} :=& \frac{v_2(1-2v_1)}{v_1+v_2-2v_1v_2},\\ \mathbf{p}^{north} :=& (0, 0, \frac{1-2v_m+2v_m^2}{2v_m-1}, 1)\ ,\\ \sigma^{north} :=& \frac{(1-v_{m-1})(2v_m-1)}{v_{m-1}+v_m-2v_{m-1}v_m},\end{aligned} \tag{14}$$

then the following construction of free-form $G^1$ spline caps defaults to the sphere. We generalize $\mathbb{s}^{-1}$ by setting

$$\begin{aligned}\mathbb{q} :=& (\mathbb{q}_1, \mathbb{q}_2, \mathbb{q}_3, \mathbb{q}_4),\\ \mathbb{q}_k :=& q_{k0} + q_{k1}x + q_{k2}y + q_{k3}(x^2+y^2),\end{aligned} \tag{15}$$

with, of yet, undetermined coefficients $q_{kl}$, and form, for the south pole (cf. Fig. 12),

$$\mathbb{q}(\rho(u, 0(1-\tilde{v}) + v_1\tilde{v})), \tag{16}$$

replace the cos-sin-pairs by rational quadratic splines and remove the common denominator of the 4-tuple. This yields bi-quadratic expansion (bi-2 jet) $\partial^2\mathbf{f}^{pole}$ illustrated in Fig. 13 (a) in red. We determine the coefficients $q_{kl}$ to best match, in the two-norm, for each of the four coordinates separately, the Bézier coefficients of the 1-jet $\partial\mathbf{f}^{body}$ (black disks in Fig. 13 (a)) by the corresponding coefficients of $\partial^2\mathbf{f}^{pole}$ (red disks). For example, $\partial\mathbf{f}^{body}$ near the south pole is represented by the points $\hat{\mathbf{b}}_{rs}^{i1} := w_{rs}^{i1}\mathbf{b}_{rs}^{i1}$, $r = 0, 1, 2$, $s = 1, 2$, with $i$ the circular index. (After projection to $\mathbb{R}^3$ the points $\hat{\mathbf{b}}_{r0}^{pole,i}$ collapse to form the pole.) As a reparameterization of a quadratic, the cap is infinitely smooth at the pole, but typically does not join smoothly

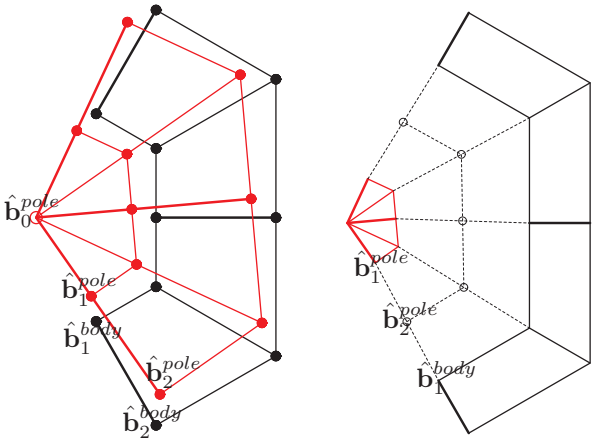


(a) $\partial^2\mathbf{f}^{pole}$ red, $\partial\mathbf{f}^{body}$ black (b) 2 patch strips

Fig. 13. Capping construction: we denote by $\hat{\mathbf{b}}_s^{pole}$ the $s$th circular sequence of coefficents $\hat{\mathbf{b}}_{rs}^{pole,i}$, with $r = 0, 1, 2$ and $i$ the circular index. (a) Overlapping expansions $\partial\mathbf{f}^{body}$ and $\partial^2\mathbf{f}^{pole}$; (b) from 1-jets to two $C^1$-connected strips of patches.

with $\mathbf{f}^{body}$. A simple remedy is to build the cap from two patch strips, one extending the body and the other surrounding the pole (cf. Fig. 13 (b)).

**2-Strip Construction.** Removing the coefficent layer $\hat{\mathbf{b}}_2^{pole}$, we truncate $\partial^2\mathbf{f}^{pole}$ to $\partial\mathbf{f}^{pole}$. We scale $\partial\mathbf{f}^{pole}$ and $\partial\mathbf{f}^{body}$ by $\frac{1}{2}$ in $\tilde{v}$, the radial direction, see Fig. 13 (b):

$$\hat{\mathbf{b}}_1^{pole} := \frac{1}{2}\hat{\mathbf{b}}_0^{pole} + \frac{1}{2}\hat{\mathbf{b}}_1^{pole}\ ,\ \hat{\mathbf{b}}_1^{body} := \frac{1}{2}\hat{\mathbf{b}}_2^{body} + \frac{1}{2}\hat{\mathbf{b}}_1^{body}.$$

We then join both strips parametrically $C^1$ as 4-tuples in the $\tilde{v}$ direction by setting

$$\hat{\mathbf{b}}_2^{pole} := \frac{1}{2}\hat{\mathbf{b}}_1^{pole} + \frac{1}{2}\hat{\mathbf{b}}_1^{body}\ ,\ \hat{\mathbf{b}}_0^{body} := \hat{\mathbf{b}}_2^{pole}\ .$$

By construction the patches join $G^1$ in the circular direction. Since the map $\mathbb{q}$ can in particular represent the inverse stereographic projection $\mathbf{s}^{-1}$, the cap construction completes a sphere if the data $\mathbf{f}^{body}$ come from a sphere.

An analoguous capping procedure applies also to the elliptic paraboloid and two-sheeted hyperboloid (see the small golden caps in Fig. 22).

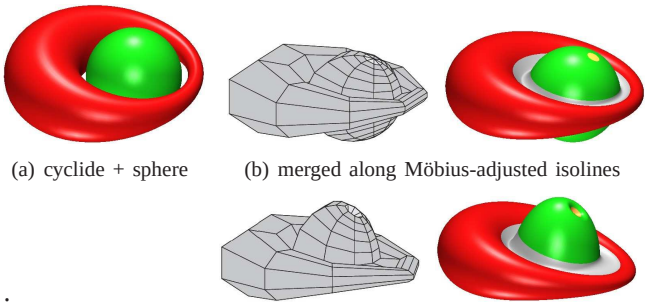

(a) cyclide + sphere (b) merged along Möbius-adjusted isolines

(c) alternative design

Fig. 14. Merging cyclide and sphere whose iso-lines have been adjusted by a Möbius transformation.

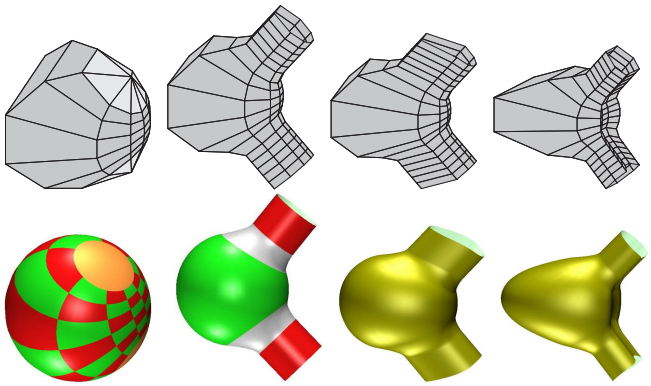

(a) exact sphere (b) $G^1$ join with (modified) cylinders

Fig. 15. Möbius-reparameterized sphere merged with cylinders.

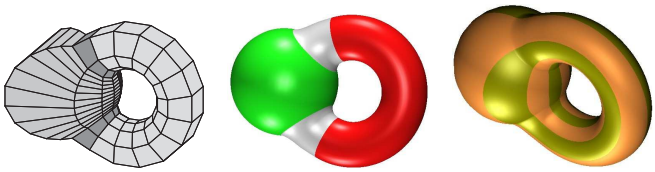

(a) control mesh (b) sphere + torus (c) iso-parameter lines

Fig. 16. Möbius-reparameterized sphere and torus.

**Design using Möbius Transformations.** To join a cyclide with a sphere, as illustrated in Fig. 14, a Möbius transformation needs to be applied. This changes the location of the poles – otherwise cyclide iso-lines would not match up with sphere-isolines. Similarly, such adjustment is needed in Fig. 15. To adjust the poles, we use the Möbius transformation $M(z) := \frac{z+b}{bz+1}$, $b \in \mathbb{R}$ that move the north pole to $\left(\frac{2b}{1+b^2}, 0, \frac{1-b^2}{1+b^2}\right)$ and the south pole to $\left(\frac{2b}{1+b^2}, 0, -\frac{1-b^2}{1+b^2}\right)$. We apply it in the form $\mathbb{s} \circ M \circ \mathbb{s}^{-1}$.

In general, we compose $\mathbb{q} \circ M \circ \rho$ to obtain for each coordinate (hence dropping the index $k$)

$$\begin{aligned}\mathbb{q} :=& q_0 b^2 + q_1 b + q_3 + \big(q_1\mathsf{c} + q_2\mathsf{s} - 2q_3 \\ &+ 2(q_0\mathsf{c} - q_1 + q_3\mathsf{c})b - (2q_0 - q_1\mathsf{c} + q_2\mathsf{s})b^2\big)v \\ &+ \big(q_0 - q_1\mathsf{c} - q_2\mathsf{s} + q_3 - 2(q_0\mathsf{c} - q_1 + q_3\mathsf{c})b \\ &+ (q_0 - q_1\mathsf{c} + q_2\mathsf{s} + q_3)b^2\big)v^2,\end{aligned}$$

where $\mathsf{c} := \cos u$, $\mathsf{s} := \sin u$. With the scalars $\beta_i$, $\sigma^{south}$ and $\sigma^{north}$ unchanged,

$$\begin{aligned}\mathbf{p}^{south} :=& (2b, 0, \frac{(1-b^2)(1-2v_1+2v_1^2)}{2v_1-1}, b^2+1), \\ \mathbf{p}^{north} :=& (2b, 0, \frac{(1-b^2)(1-2v_m+2v_m^2)}{2v_m-1}, b^2+1)\end{aligned} \tag{17}$$

generalizes (14). Fig. 14, 15 and 16 show examples of models using Möbius-adjusted parameterizations.

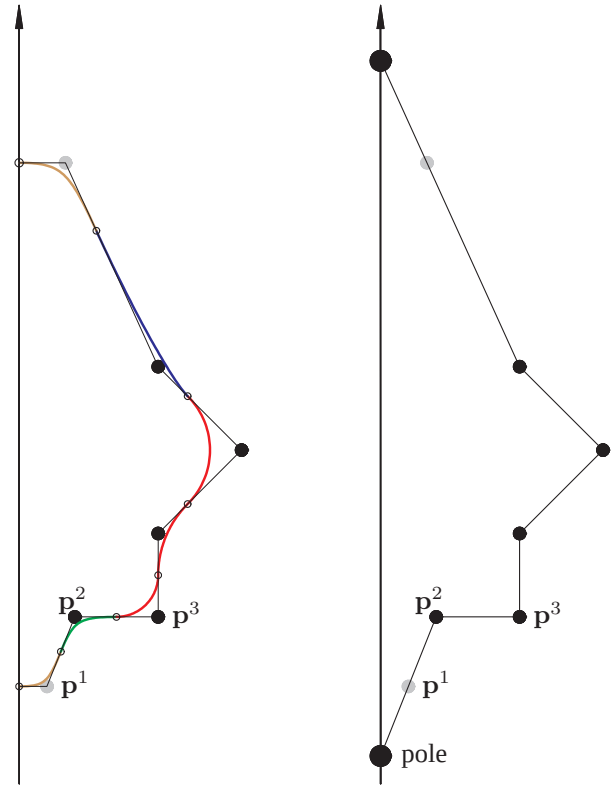


Fig. 17. (*left*) Profile $G^1$ spline: circles (red), ellipse (blue), hyperbolas (green and gold). (*right*) Its control polygon transformed into form suitable for free-form polar modeling; (cf. Fig. 12(d)).

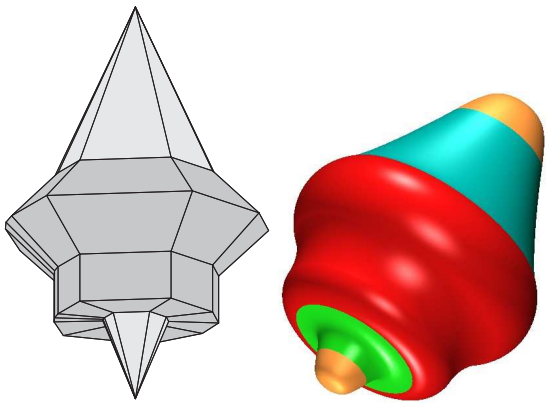

Fig. 18. Surface of revolution corresponding to the profile and axis of Fig. 17.

### 6.1. *Free-form surfaces of revolution*

Our goal now is to turn the earlier construction of surfaces of revolution into one that can be freely modified also at the poles.

For smoothness at the poles, the pole-most curve segments must meet the axis of rotation orthogonally (cf. Fig. 17). We proceed as in the earlier construction of surfaces of revolution: we derive a polar control mesh from the control polygon of the profile spline, assuming that the line through the control points $\mathbf{p}^1$ and $\mathbf{p}^2$ intersects the $z$-axis. For example, if $\mathbf{p}^i := (x_i, 0, z_i)$ then

$$\mathbf{p}^{pole} := \Big(0, 0, \frac{z_1 x_2 - x_1 z_2}{x_2 - x_1}\Big) \tag{18}$$

and we can calculate the parameter $\sigma$ from $\mathbf{p}^1 := (1-\sigma)\mathbf{p}^2 + \sigma\mathbf{p}^{pole}$. Then, for all $i$, $\mathbf{p}^{i1} := (1-\sigma)\mathbf{p}^{i2} + \sigma\mathbf{p}^{pole}$ and (10) defines all other control points $\mathbf{p}^{ij}$.

For the capping, however, unless we enforce that the quadratic expansion of the end of the profile curves remain symmetric with respect to the $z$-axis, we can no longer assume that the curve expansions in pole vicinity can be parameterized as part of a single quadratic map. We therefore use only a linear $\mathbb{q}$,

$$\mathbb{q} := (\mathbb{q}_1, \mathbb{q}_2, \mathbb{q}_3, \mathbb{q}_4),\ \mathbb{q}_k(s,t) := q_{k0} + q_{k1}s + q_{k2}t$$

and form, at the south pole, the map

$$q_{k0}B_0(v) + (q_{k0} + q_{k1}\cos u + q_{k2}\sin u)\ddot{w}_1^1 B_1(v). \tag{19}$$

(The map at the north pole replaces $v$ by $1-v$ and $w_1^1$ by $w_1^m$.) As in the earlier constructions, we replace $\cos u$, $\sin u$ by rational quadratic splines and remove the common denominator of the 4-tuple. This yields the first-order expansion $\partial\mathbf{f}^{pole}$. As in the construction of General Polar Caps, we determine the coefficients $q_{kl}$ by minimizing the two-norm distance between the Bézier coefficients $\hat{\mathbf{b}}_1^{pole}$ and $\hat{\mathbf{b}}_1^{body}$ and then apply the 2-Strip Construction.

The cap is tangent plane continuous at the pole, since $\hat{\mathbf{b}}_0^{pole}$ and $\hat{\mathbf{b}}_1^{pole}$ are in the plane defined by the linear map $\mathbb{q}$. And, if the data $\hat{\mathbf{b}}^{body}$ come from surface of revolution, the cap construction completes it. Fig. 18 shows the standard surface of revolution obtained from the profile and axis of Fig. 17. Fig. 19 illustrates the advantage of our new construction over standard surfaces of revolution: based on the circle segmentation Fig. 19 shows a localized re-design of Fig. 18.

The close relation of surfaces of revolution and the sphere construction at the beginning of Section 6 raises the question: why not construct free-form spheres directly as surfaces of revolution? While such a construction is clearly possible, it reduces the design flexibility since now the Möbius transformation can only be applied to the circular direction.

## 7. From $G^1$ in $\mathbb{R}^3$ to $C^1$ in $\mathbb{P}^3$

It has been argued, e.g. in [Zhe09], that for lofting, $C^1$ continuity in homogeneous space is more appropriate than $G^1$ continuity in $\mathbb{R}^3$. We are interested in such a reparameterization at the boundaries of multi-sided blends. The literature offers many such constructions. Their details are not important here, only that the simpler constructions prefer $C^1$-connected surface layers surrounding the multi-sided gap. We therefore focus on converting our $G^1$ patchwork, arising from the $(\cos, \sin)$-pair conversion to rational biquadratic form, to a patchwork that is $C^1$ in $\mathbb{P}^3$ along the gap boundary. For example, the design of

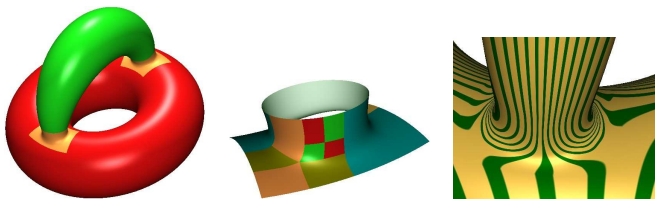

(a) torus+cyclide (b) patch layout (c) highlight lines

Fig. 20. $G^1$ surface (a) built from a torus and a cyclide handle using (b) multiple patches. (c) shows the quality of the transition.

Fig. 20 requires $n = 5$-sided blends, uniformly laid out. One possible switch from our $G^1$ join in $\mathbb{R}^3$ to a $C^1$ join in $\mathbb{P}^3$ can be achieved as in [BP97,Fan02]. This approach allows a construction, itself outside the scope of this paper, that uses $n \times 2 \times 2$ patches of degree bi-4 as shown in Fig. 20 (b). Alternatively, for the same layout, we can even support a bi-3 construction such as [FP11] as follows. We transform the rational bi-2 patches, representing the cos-sin-pairs with uniform opening angle, into $2\times 2$ bi-3 splines that are $C^1$ connected in homogeneous space, rather than $G^1$ in Euclidean space. First we consider the curve construction, then form the tensor-product.

*Curve Construction:* We adapt the approach of [Zhe09] since it originally does not apply to closed curves. Given the quadratic curve with $w_0^i = w_2^i = 1$, $w_1^i := \omega$, in homogeneous form,

$$\mathbf{f}^i(u) := \Big(\sum_k^2 w_k^i \mathbf{b}_k^i B_k^2(u)\ ,\ \sum_k^2 w_k^i B_k^2(u)\Big), \tag{20}$$

we create, by reparameterization, pre-scaling to cancel common denominators and linearly post-scaling that increases the degree to 3, a left piece,$\mathbf{f}_l^i$ and a right piece $\mathbf{f}_r^i$

$$\begin{aligned}
\mathbf{f}_l^i(u) &:= ((1-u)+\mu u)^2 \mathbf{f}^i\Big(\frac{\frac{1}{2}\mu u}{(1-u)+\mu u}\Big)(1-u+\eta u),\\
\eta &:= \frac{\mu}{3\mu - 2},\\
\mathbf{f}_r^i(u) &:= (\mu(1-u)+u)^2 \mathbf{f}^i\Big(\frac{\frac{1}{2}\mu(1-u)+u}{\mu(1-u)+u}\Big)(\eta(1-u)+u).
\end{aligned} \tag{21}$$

The explicit Bézier coefficients and weights of $\mathbf{f}_l^i$ and $\mathbf{f}_r^i$ are

$$\begin{aligned}
&\mathbf{b}_{l,j}^i := \sum_{k=0}^2 \tau_{jk}\mathbf{b}_k^i,\ \mathbf{b}_{r,j}^i := \sum_{k=0}^2 \tau_{jk}\mathbf{b}_{2-k}^i,\\
&w_{l,0}^i := 1,\ w_{l,1}^i := \frac{d_0\mu}{d_1},\ w_{l,2}^i := \frac{d_2\mu^3}{2d_1},\ w_{l,3}^i := w_{l,2}^i,\\
&w_{r,j}^i = w_{l,3-j}^i,
\end{aligned} \tag{22}$$

where

$$\begin{aligned}
&d_0 := -1 + 3\mu + 3\mu\omega - 2\omega,\ d_1 := 3\mu - 2\ ,\ d_2 := 1+\omega,\\
&\tau_{00} := 1\ ,\ \tau_{01} = \tau_{02} := 0\\
&\tau_{10} := \frac{3\mu - 1}{d_0},\ \tau_{11} := \frac{d_1\omega}{d_0}, \tau_{12} := 0,\\
&\tau_{20} := \frac{3\mu + 2}{6d_2\mu},\ \tau_{21} := \frac{\omega}{d_2},\ \tau_{22} := \frac{d_1}{6d_2\mu},\\
&\tau_{30} := \frac{1}{2d_2}, \tau_{31} := \frac{\omega}{d_2},\ \tau_{32} = \tau_{30}.
\end{aligned} \tag{23}$$

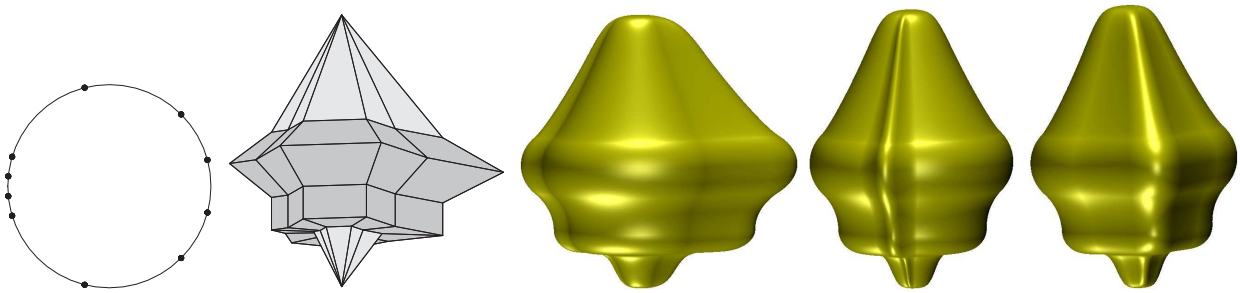

Fig. 19. Localized free-form re-design of the surface of revolution Fig. 18 based on the designer's circle segmentation.

Theorem 3 states that this curve construction yields homogeneous $C^1$ transitions as is verified by substitution.

**Theorem 3** *For any $\mu$, $\mathbf{f}_l^i$ and $\mathbf{f}_r^i$ join $C^1$ in homogeneous space. If $\mu$ is any (real) root of the equation $3(1+\omega)\mu^2-2(5+\omega)\mu+6=0$ then also $\mathbf{f}_r^{i-1}$ and $\mathbf{f}_l^i$ join $C^1$ in homogeneous space: $\mathbf{f}_l^i(0)=\mathbf{f}_r^{i-1}(1)$ and $(\mathbf{f}_l^i)'(0)=(\mathbf{f}_r^{i-1})'(1)$.*

Analoguously, to prepare $C^1$ data for the multi-sided construction, we transform biquadratic $G^1$ splines to bicubic $C^1$ splines in homogenous space by tensoring (22).

## 8. Remarks and Conclusions

For *curve design*, the simplicity and flexibility of the construction and the rational $G^1$ spline's ability to include a variety of conic shapes in one smooth whole stands in contrast to the recent, more complicated non-linear curve subdivision algorithms that are limited to reproducing just one conic at a time.

One goal of the proposed work-flow, especially for surfaces, is to *initialize the design and overall layout* with a predictable shape of high quality. In the modification step, Fig. 4 (c), the designer has the freedom to create any number of more intricate additional features, just as for standard NURBS.

Our rational $G^1$ splines represent a *trade-off in flexibility*. On one hand, they are a subset of all smooth bi-quadratic patchworks, as discussed under Limitations in Section 5; on the other hand, they are more flexible than highly specialized families of (bi-)quadratics, such as cyclide patches [Pra89], which provide explicit offsets, and sphere-and-hyperboloid 'skin surfaces' [Ede99] that are specialized to modeling molecules. Such special purpose spline families are too restrictive for use in general design, while the many examples shown in this paper show a rich set of rational biquadratic shapes that can locally replicate the specialized splines.

Villarceau-parameterization, stretching and Möbius maps yield alternative distributions of shape handles for the same basic shape, namely the torus, the cylinder and the sphere.

This paper focused on construction at the mathematical level. In practice, the actual design interface is crucial but we do not discuss it here, since such an interface must surely vary from CAD package to CAD package. Our original work-flow used Maple to generate the patch and the opensource package *Bezierview* [Bez] for display. We are modifying this to use *blender*, C++ and *Bezierview*.

This paper focused on a simple bi-quadratic construction. The corresponding bi-cubic rational $G^2$ construction [KP11] is more complex. At the moment, it does not seem practical to derive analogous rational splines of degree higher than bi-cubic for yet smoother constructions. Conversely, the simplicity of the presented $G^1$ construction recommends itself where the low polynomial degree is advantageous and first-order smoothness suffices.

## References


[Bar93] Brian A. Barsky. Rational beta-splines for representing curves and surfaces. *IEEE Comp Graph and Appl*, 13(6):24–32, 1993.

[Bez] Bezierview. http://www.cise.ufl.edu/research/SurfLab/bview/.

[Boe87] Wolfgang Boehm. Rational geometric splines. *Computer Aided Geometric Design*, 4(1-2):67–77, July 1987.

[BP97] Claudia Bangert and Hartmut Prautzsch. Circle and sphere as rational splines. *Neural, Parallel and Scientific Computations*, (5):153–162, 1997.

[DMP93] Debasish Dutta, Ralph R. Martin, and Michael J. Pratt. Cyclides in surface and solid modeling. *IEEE Computer Graphics and Applications*, 13(1):53–59, January 1993.

[Ede99] Herbert Edelsbrunner. Deformable smooth surface design. *Discrete & Computational Geometry*, 21(1):87–115, 1999.

[Fan02] Lian Fang. A rational quartic Bézier representation for conics. *Computer Aided Geometric Design*, 19(5):297–312, 2002.

[Far88] Gerald Farin. *Curves and Surfaces for Computer Aided Geometric Design: A Practical Guide*. Academic Press, 1988.

[Far06] Gerald E. Farin. Rational quadratic circles are parametrized by chord length. *Comp Aided Geom Design*, 23(9):722–724, 2006.

[FP11] Jianhua Fan and Jörg Peters. Smooth bi-3 spline surfaces with fewest knots. *Computer Aided Design*, 43(2):180–187, Feb 2011.

[GB88] Ronald N. Goldman and Brian A. Barsky. Beta continuity and its application to rational beta-splines. Technical Report CSD-88-442, University of California, Berkeley, August 1988.

[Joe89] Barry Joe. Multiple-knot and rational cubic beta-splines. *ACM Transactions on Graphics*, 8(2):100–120, 1989.

[KP07] K. Karčiauskas and J. Peters. Surfaces with polar structure. *Computing*, 79:309–315, March 2007.

[KP11] K. Karčiauskas and J. Peters. Rational bi-cubic $G^2$ splines for design with basic shapes. In *Symposium on Geometry Processing*, pages x–x+6, 2011.

[PBP02] Hartmut Prautzsch, Wolfgang Boehm, and Marco Paluszny. *Bézier and B-spline techniques*. Springer Verlag, 2002.

[Pra89] M. Pratt. Applications of cyclide surfaces in geometric modelling. In D. C. Handscomb, editor, *The Mathematics of Surfaces III*, pages 405–428. Clarendon Press, 1989.

[Zhe09] Jianmin Zheng. $C^1$ NURBS representations of $G^1$ composite rational Bézier curves. *Computing*, 86(2–3):257–268, October 2009.

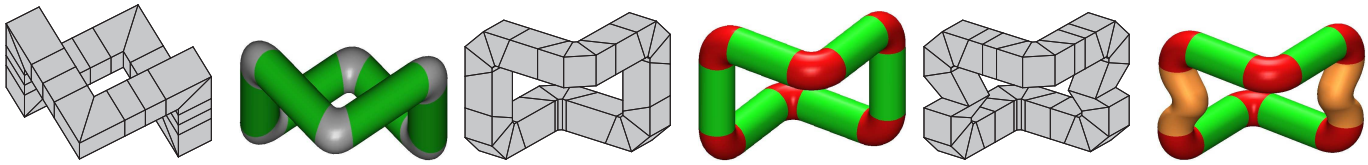

(a) cylinders joined (b) cylinders+tori (c) cylinders+tori + free-form

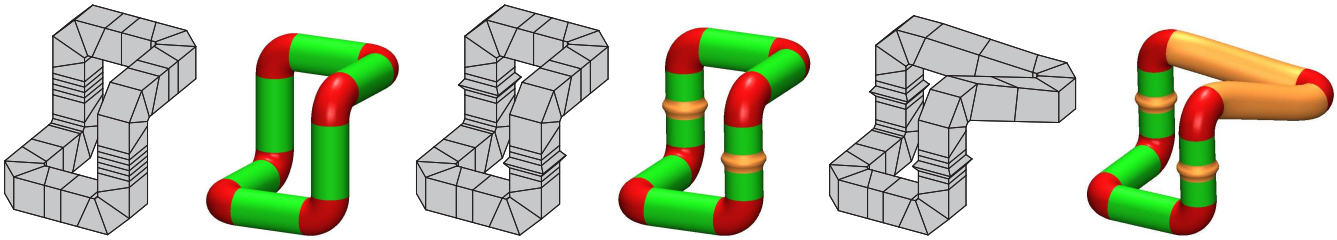

(d) cylinders+tori (e) cylinders+tori+ free-form (f) cylinders+tori+free-form

Fig. 21. Design with cylinders: (a) cylinder pieces (green) are joined in a $G^1$ spline with transitions (grey). (b) Transitions using torus pieces (red) defined by two segments. (c) Free-form sections are in orange. (d) Minimal meshes are not always suitable for subtle design. But cylinders can easily be segmented more finely, without changing the geometry, to enable the design variants (e) and (f).

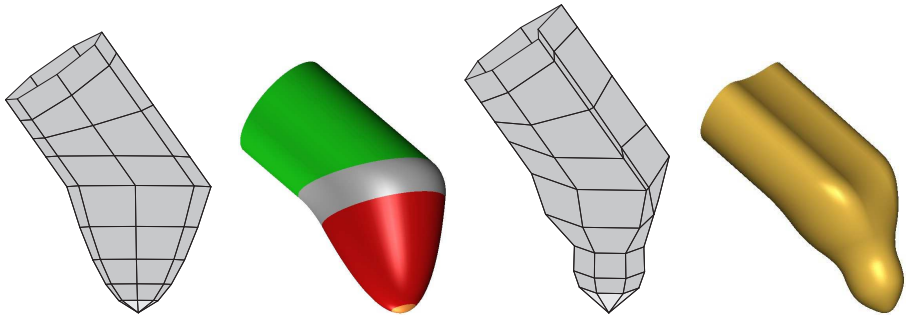

(a) cylinder + elliptic paraboloid (b) design variant

(c) circular two-sheeted hyperboloid + elliptic cylinder + circular cone (d) design variant

Fig. 22. Designs with quadrics.

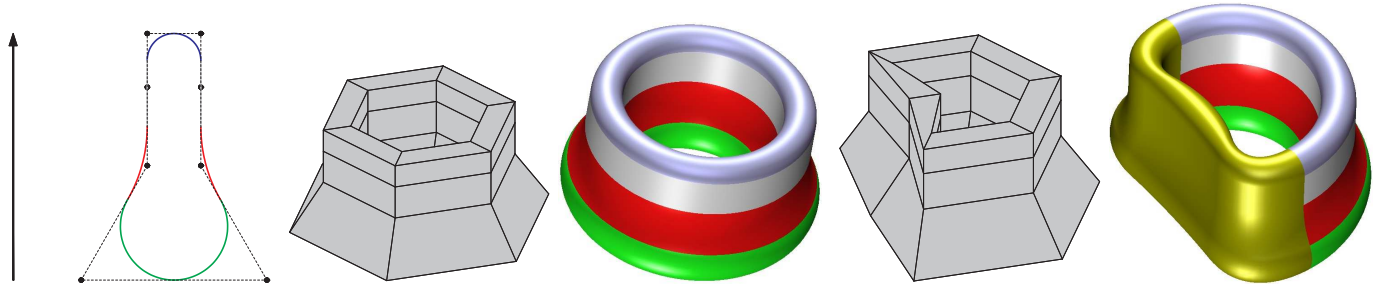

(a) axis and profile curve (b) initial design (c) free-form design

Fig. 23. Design with surfaces of revolution: (a) $z$-axis and profile, (b) the profile's sweep surface about the $z$-axis and (c) free-form design preserving part of the surface of revolution.